Microscale Thermophysical Engineering, 9:137–153

ISSN: 1089-3954 print/1091-7640 online
DOI: 10.1080/10893950590945021

Taylor & Francis
Taylor & Francis Group

VALIDATION OF A SECOND-ORDER SLIP MODEL FOR DILUTE GAS FLOWS

Nicolas G. Hadjiconstantinou
Mechanical Engineering Department, Massachusetts Institute of Technology, Cambridge, Massachusetts, USA

We present an extensive comparison between direct Monte Carlo simulations and the predictions of the Navier-Stokes description coupled to a recently proposed second-order slip model for hard sphere gases. Two one-dimensional, time-dependent channel flows are considered. In both cases excellent agreement is found between molecular simulation and the proposed model well into the transition regime for both the velocity and stress fields. The excellent quantitative agreement extends, approximately, to a Knudsen number based on the channel width of 0.4. The transient nature of the flows suggests that the slip model, despite its (quasi-) steady origins, remains reliable as long as the evolution timescale is long compared to the molecular collision time. Our discussion elucidates the effect of the Knudsen layer, a kinetic "boundary layer" in the vicinity of walls that needs to be superposed to the Navier-Stokes component of the flow in order to obtain the complete flow solution. The existence of this kinetic boundary layer, whose importance grows with increasing Knudsen number and which ultimately renders the Navier-Stokes component insufficient to describe the flow, implies that special care is needed in interpreting slip-flow flowfields.

Keywords Navier-Stokes, Boltzmann, second-order slip, Knudsen layer, small-scale flows

Second-order slip models can, in some cases, extend the range of applicability of the Navier-Stokes* description around and beyond Kn $\cong 0.1$ where the accuracy of first-order slip models begins to deteriorate [1, 2]. Given the simplicity and negligible cost of Navier-Stokes solutions compared to molecular simulations, accurate second-order slip models are very desirable [3].

Although a number of researchers [3] have proposed second-order slip laws of the form

$$\hat{u}|_{wall} - u_w = \alpha\lambda \left.\frac{\partial \hat{u}}{\partial \eta}\right|_{wall} - \beta\lambda^2 \left.\frac{\partial^2 \hat{u}}{\partial \eta^2}\right|_{wall} \tag{1}$$

The author thanks Dr. M. Gallis for helpful discussions.

Address correspondence to Nicolas G. Hadjiconstantinou, Mechanical Engineering Department, Massachusetts Institute of Technology, Cambridge, MA 02139. E-mail: ngh@mit.edu

*The slip model discussed here is based on a kinetic linear theory that requires very small Reynolds numbers. The term "Navier-Stokes" is used here to generally denote the continuum hydrodynamic description with viscous closures appropriate to the Kn $\ll 1$ limit.

NOMENCLATURE

i	$\sqrt{-1}$
k	Boltzmann's constant
Kn	Knudsen number $= \lambda/L$
L	distance between walls
m	molecular mass
R	Gas constant $= k/m$
t	time
T	temperature
T	oscillation period
u	gas velocity $= \hat{u} + u_{KN}$
u_b	bulk velocity
u_b^{DSMC}	bulk velocity calculated by DSMC
u_{KN}	Knudsen layer component of gas velocity
$\hat{u}$	Navier-Stokes component of gas velocity
u_w	wall velocity
$u\|_{wall}$	gas velocity at the wall
U	wall velocity amplitude
y	transverse coordinate
y_w	wall location

Greek Symbols

α	first-order slip coefficient
β	second-order slip coefficient
γ	ratio of specific heats
δ	$\beta - \xi$
ε	molecular collision frequency $= 1/\tau_c$
ζ	$\sqrt{i\phi}$
η	coordinate normal to the wall
λ	molecular mean free path
μ	coefficient of viscosity
ν	kinematic viscosity $= \mu/\rho$
ξ	0.296
ρ	mass density
τ	stress
τ_c	molecular collision time
τ_w	shear stress at the wall
τ_w^*	$\tau_w/(\mu U/L)$
ϕ	Stokes number $= \sqrt{\omega L^2/\nu}$
ω	oscillation frequency

as "obvious" extensions of the first-order slip law

$$\hat{u}|_{wall} - u_w = \alpha\lambda \left.\frac{\partial \hat{u}}{\partial \eta}\right|_{wall} \tag{2}$$

use of such models can only be justified by a rigorous asymptotic analysis of the Boltzmann equation. Such analysis by Cercignani [4], albeit for a BGK gas, shows that in steady, one-dimensional flows the appropriate second-order boundary condition is of the form of Equation (1). Within the asymptotic analysis, slip flow boundary conditions such as Equations (1) and (2) provide effective boundary conditions for $\hat{u}$, the Navier-Stokes component of the true flowfield, whereas in the near-wall regions a kinetic boundary layer, known as Knudsen layer, needs to be superposed to the former to capture the true solution of the Boltzmann equation; i.e., $u = \hat{u} + u_{KN}$ with $u_{KN} \to 0$ as $(y - y_w)/\lambda \to \infty$ [5, 6]. However, the "effective" thickness of the Knudsen layer, based on the decay of u_{KN} to a few percent of its maximum value, is approximately 1.5λ [5]. Cercignani's study shows that the contribution of the Knudsen layers to the flow is such that the average flow velocity differs from the slip-corrected Navier-Stokes approximation to $O(\text{Kn}^2)$. Thus, while for $\text{Kn} \leq 0.1$ using only $\hat{u}$ to describe the flow is typically sufficient, for $\text{Kn} \geq 0.1$ and when using second-order slip boundary conditions in particular, Knudsen layers need to be quantitatively taken into account. The existence of the Knudsen layer also implies that a successful second-order slip model is one that does not agree with Boltzmann equation solutions within 1.5λ from the walls. This explains why attempts toward determining β by fitting direct simulation Monte Carlo (DSMC) solutions in the entirety of the simulation domain have not led to a predictive model with no adjustable parameters.

Based on these observations and Cercignani's analysis, the author, in a recent paper [7], has proposed a second-order slip model for the hard sphere gas, with no adjustable coefficients. The model synthesizes elements of the BGK asymptotic theory for steady flows (pioneered by Cercignani [4] and generalized by Sone [6]) to construct a second-order slip framework, but substitutes the BGK slip coefficients with values appropriate for the hard sphere gas. As will be seen, this improvement holds the key to making second-order slip-flow theory useful, since now agreement with realistic Boltzmann simulations and physical experiments can be sought and demonstrated. In fact, as is also discussed, the second-order slip model in its hard sphere form is able to explain recent experimental measurements. The ability to connect to simulation results and experiments is of great importance; it is our belief that the inability of the second-order slip model in its BGK form to provide such a connection is one of the primary reasons for the lack of interest in the original (BGK) version of the theory. The fact that original experiments misinterpreted the model, thus exaggerating the discrepancy between the experimental results and the theoretical (BGK) description, has certainly contributed to this [7].

In this article we hope to provide a simple exposition of the second-order slip-flow theory but also to validate the hard sphere version proposed by the author [7]. We feel that this validation is required since in proposing this hard sphere model the applicability of the BGK second-order steady slip-flow framework to both steady and unsteady hard sphere gas flows was conjectured. The model has already been found [7] to be in excellent agreement with direct Monte Carlo solutions of the Boltzmann equation for pressure driven flows up to Kn ≈ 0.4 (see Figure 1).

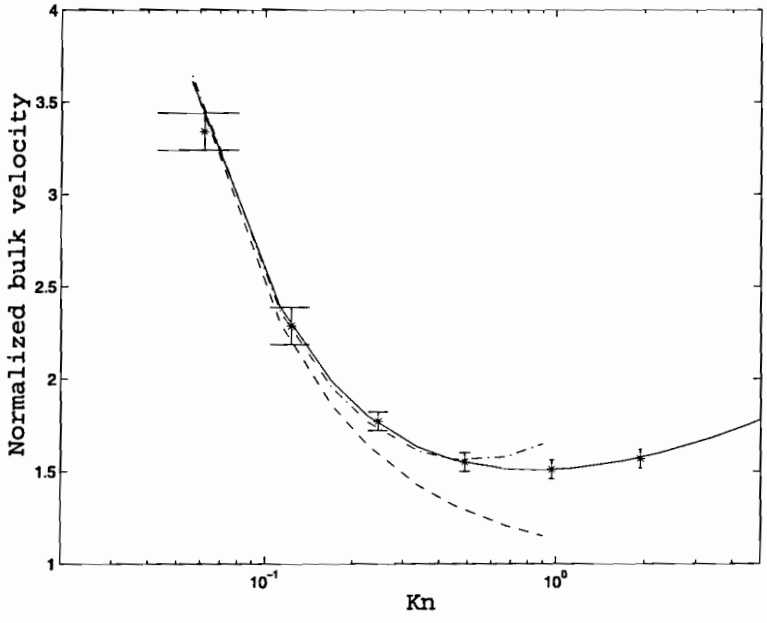

Figure 1. Bulk velocity in pressure driven flow, u_b, normalized by $(-\frac{1}{P}\frac{dP}{dx}L\sqrt{\frac{RT}{2}})$. The solid line denotes numerical solution of the linearized Boltzmann equation [20]; the stars denote DSMC results; the dashed line denotes a first-order slip model; and the dash-dotted line denotes the second-order slip model of this article.

Below, we obtain solutions to two one-dimensional time-dependent problems using this model. The results are compared to direct Monte Carlo solutions of the Boltzmann equation. Our results demonstrate that it is indeed possible to capture the flow and stress field for arbitrary one-dimensional flows up to Kn $\cong 0.4$ using a rigorous second-order slip model (with no adjustable parameters); validation in higher dimensions has yet to be performed. In higher dimensions the second-order slip term is significantly more complex. Additionally, when flow normal to the wall exists, velocity slip normal to the wall is also present; BGK examples can be found in Sone [6]. Terms involving wall curvature also appear (these were neglected in Cercignani [4]); these explain the difference in the second-order slip coefficient observed in pressure-driven flows in tubes compared to the same flow in two-dimensional channels.

Accurate description of the stress field without additional adjustable parameters is, in fact, a basic requirement since the assumption that the stress is given by the viscous constitutive law is implicit in the use of a slip-corrected Navier-Stokes description. Within the asymptotic theory, this is manifested by the fact that the stress field is not subject to a Knudsen layer correction [6].

This article demonstrates that while the slip model continues to provide accurate descriptions of the stress field as the Knudsen number increases, the fraction of the domain over which $\hat{u}$ describes the true flowfield (u) becomes smaller because Knudsen layers penetrate increasingly larger parts of the domain. However, by accounting for the difference $u - \hat{u} = u_{KN}$, the model is able to accurately predict the average over the domain (bulk) velocity. As shown below, this correction seems to provide a resolution of the long-standing discrepancy between experimental data and second-order slip model predictions; in particular, this model explains the recent experimental findings of Maurer et al. [8], who measured the second-order slip coefficient in two-dimensional pressure-driven channel flow. Finally, our results demonstrate that the slip model can be used in time-dependent problems as long as the characteristic evolution timescale is longer than the molecular collision time.

In this work we have used the hard sphere gas model; this model has been shown to provide a good approximation to real isothermal flows [9]. Once the methodology for developing second-order slip models is validated, second-order slip models for other interaction models [10] can be developed using the approach previously described [7].

SECOND-ORDER SLIP MODEL FOR THE HARD SPHERE GAS

In one-dimensional flows, the hard sphere second-order slip model reduces to Equation (1) with $\alpha = 1.11$ and $\beta = 0.61$. The model also includes a method for quantitatively accounting for the contribution of the Knudsen layer without solving the Boltzmann equation. The contribution of the Knudsen layer can be accounted for in an average sense; i.e., when calculating the bulk flow velocity. In a one-dimensional geometry ([0, L]), the average (bulk) flow velocity is given by

$$u_b = \frac{1}{L}\int_0^L u dy = \frac{1}{L}\int_0^L \left[\hat{u} + \xi\lambda^2 \frac{\partial^2 \hat{u}}{\partial y^2}\right] dy \tag{3}$$

where the second term in the last equality gives the contribution of the Knudsen layer to the bulk flow. For a hard sphere gas $\xi = 0.296$ [7].

A direct consequence of the above relation is that in Poiseuille-type flows where the velocity curvature is a constant (in the Navier-Stokes approximation), experimental measurement of the flow rate (bulk flow velocity) yields an "effective" second-order slip coefficient $\beta - \xi$ [7]. In other words, while the average value of a Poiseuille flow profile subject to second-order slip of the form (1) is given by

$$\hat{u}_b = \frac{1}{L}\int_0^L \hat{u}dy = -\frac{L^2}{2\mu}\frac{dP}{dx}\left(\frac{1}{6} + \alpha \mathrm{Kn} + 2\beta \mathrm{Kn}^2\right)$$

where dP/dx is the pressure gradient driving the flow, the true bulk flow speed (as inferred by an experiment measuring the flow rate) is given by Equation (3), which leads to

$$u_b = \frac{1}{L}\int_0^L \left(\hat{u} + \xi\lambda^2\frac{\partial^2\hat{u}}{\partial y^2}\right)dy = -\frac{L^2}{2\mu}\frac{dP}{dx}\left(\frac{1}{6} + \alpha \mathrm{Kn} + 2\delta \mathrm{Kn}^2\right)$$

with $\delta = \beta - \xi$. As shown in a previous work [7] and Figure 1 of this article, the above equation captures the flow rate in isothermal pressure-driven flow accurately up to $\mathrm{Kn} \approx 0.4$. Most importantly, this fact explains the findings of recent experiments [8] on helium and nitrogen flow in small-scale channels; these experiments find the second-order slip coefficient to be approximately 0.25 ± 0.1. Of course, since the slip coefficient was determined by measuring the flow rate, these experiments were in fact determining the effective second-order slip coefficient δ (and not β, as they thought), which is in good agreement with the value $\delta = 0.31$ predicted by the slip model.

Discussion of Limitations

It appears that a number of the assumptions on which this model is based do not significantly limit its applicability. For example, it would be reasonable to assume that the assumption of steady flow would be satisfied by flows that appear quasistatic at some timescale. Our results suggest that this timescale is the molecular collision time; in other words, the slip model is valid for flows that evolve at timescales that are long compared to the molecular collision time, which can be satisfied by the vast majority of practical flows of interest.

The model was also derived under the assumption of flat walls and no variations in directions other than normal to the wall. Of course, approaches based on assumptions of slow variation in the axial direction, such as the widely used locally fully developed assumption or long wavelength approximation, are expected to yield excellent approximations when used for two-dimensional problems. This is verified by comparison of solutions of such problems to DSMC simulations [11] or experiments [8].

Extension of the model to higher dimensions within the BGK approximation has been considered by Cercignani [4]. Validation of this and other solutions (after they have been appropriately modified using the approach described by the author [7]) that take wall curvature, three-dimensional flowfield and non-isothermal conditions into account [6] should be undertaken. The exact conditions under which Equation (3) can be generalized also need to be clarified. While the contribution of the Knudsen layer can always be found by a Boltzmann equation analysis, the value of Equation (3) lies in the fact that it

relates this contribution to the Navier-Stokes solution and thus requires no solution of the Boltzmann equation. Finally, recall that the linearized conditions (Ma $\ll 1$) under which the second-order model is derived imply Re $\ll 1$ since Ma $\approx$ Re·Kn and Kn > 0.1. Here Ma is the Mach number and Re is the Reynolds number, based on the same characteristic length scale as Kn.

VALIDATION

In this section we use the direct simulation Monte Carlo (DSMC) method [10] to obtain solutions of the Boltzmann equation for two one-dimensional, time-dependent problems. These solutions will be used for validation of the slip model discussed above.

DSMC is a stochastic molecular simulation technique for solving the nonlinear Boltzmann equation. Consistency between DSMC solutions and solutions of the Boltzmann equation in the limit of infinitesimal discretization and large number of particles was recently shown by Wagner [12]. Quadratic convergence with cell size was shown by Alexander et al. [13], and quadratic convergence with the timestep was shown by the author [14] and Garcia and Wagner [15]. Standard DSMC procedures [10, 11] were used.

OSCILLATORY SHEAR DRIVEN FLOW

We consider a dilute gas between two infinitely long, smooth, fully accommodating walls located at $y = 0$ and $y = L$, respectively. One of the walls ($y = L$) moves sinusoidally in time with frequency ω. This problem has been studied recently [16, 17] and can be used as a validation problem since analytical solutions of it in the Navier-Stokes (NS) limit can be readily obtained. In this limit, the equation governing the gas motion is

$$\frac{\partial \hat{u}}{\partial t} = \nu \frac{\partial^2 \hat{u}}{\partial y^2} \tag{4}$$

where ν is the gas kinematic viscosity, while the second-order slip boundary condition applied to walls can be written as

$$\hat{u} = \alpha\lambda \frac{\partial \hat{u}}{\partial y} - \beta\lambda^2 \frac{\partial^2 \hat{u}}{\partial y^2} \quad \text{at} \quad y = 0 \tag{5}$$

and

$$\hat{u} - U\mathrm{Im}[\exp(i\omega t)] = -\alpha\lambda \frac{\partial \hat{u}}{\partial y} - \beta\lambda^2 \frac{\partial^2 \hat{u}}{\partial y^2} \quad \text{at} \quad y = L \tag{6}$$

The steady solution of Equation (4) subject to (5) and (6) is

$$\hat{u} = \mathrm{Im}\left[\left(A \sinh \zeta \frac{y}{L} + B \cosh \zeta \frac{y}{L}\right) \exp(i\omega t)\right] \tag{7}$$

where

$$A = \frac{U}{C + \dfrac{\alpha \mathrm{Kn}\zeta}{1 + \beta\zeta^2 \mathrm{Kn}^2} D}$$

$$B = \frac{\alpha \mathrm{Kn}\zeta}{1 + \beta\zeta^2 \mathrm{Kn}^2} A$$

$$C = \sinh\zeta + \alpha \mathrm{Kn}\zeta \cosh\zeta + \beta \mathrm{Kn}^2 \zeta^2 \sinh\zeta$$

$$D = \cosh\zeta + \alpha \mathrm{Kn}\zeta \sinh\zeta + \beta \mathrm{Kn}^2 \zeta^2 \cosh\zeta$$

$\zeta = \sqrt{i}\phi$ and $\phi = \sqrt{\omega L^2/\nu}$ is the Stokes number [16], which quantifies the effect of inertia.

We now present a comparison between DSMC solutions and solution (7) in the range $0.1 \leq \mathrm{Kn} \leq 0.4$. The frequency ($\omega$) in our simulations was chosen to be small compared to the molecular collision frequency (ε) but also sufficiently high ($\phi \gtrsim 1$) such that the flow was not in the quasistatic regime ($\phi \ll 1$) where linear velocity profiles are observed. In our simulations the wall velocity amplitude, U, was set to $0.1\sqrt{\gamma RT}$; this choice represents a reasonable balance between the requirement of high speeds for good signal-to-noise ratio [18] and low speeds for negligible compressibility, viscous heating effects, and the requirement $\mathrm{Ma} \ll 1$. For this time-periodic flow, our comparisons will focus on detailed flowfield comparisons (important for illustrating the effect of the Knudsen layer) at $t = \frac{\mathrm{T}}{2}$, where $\mathrm{T} = \frac{2\pi}{\omega}$ is the oscillation period. Due to the asymmetric nature of the flow, this time instant is not in any way special and thus there is no reason to expect the excellent agreement shown below to be limited to $t = \frac{\mathrm{T}}{2}$, especially since the model proposed is not a fit but is based on rigorous solutions of the Boltzmann equation. A second comparison with a different time-dependent flow described later demonstrates this clearly. Extensive comparisons with DSMC results for the oscillatory shear driven flow have been previously published [19].

Figure 2 shows a comparison between the DSMC results and a first- and second-order slip solution for $\mathrm{Kn} = 0.1$, $\phi = 5/\sqrt{2}$. This figure clearly shows that the first-order slip solution is already not very accurate in regions of high curvature, whereas the second-order slip solution is in excellent agreement with the DSMC result up to a distance of 1.5λ from the wall. Closer to the wall, the Knudsen layer causes the DSMC and second-order slip solutions to deviate. In fact, it is interesting to note that the discrepancy is significantly larger at $y = L$ than $y = 0$ since as predicted by Equation (3) the discrepancy depends on the local value of the curvature. Table 1 shows that Equation (3) correctly accounts for the effect of the Knudsen layer on the average velocity. It also shows that the Knudsen layer tends to make the first-order slip solution look better than it actually is.

Figure 3 shows a similar comparison for $\mathrm{Kn} = 0.2$, $\phi = 2.5/\sqrt{2}$. The effect of the Knudsen layers becomes more pronounced, especially because they now occupy approximately 60% of the physical domain. Note, however, that the second-order slip solution is in excellent agreement with the DSMC result in the remaining 40% of the domain, while the first-order slip solution clearly underestimates the amount of slip present. Table 1 provides further evidence that the second-order slip model accurately captures the true physics of the flow.

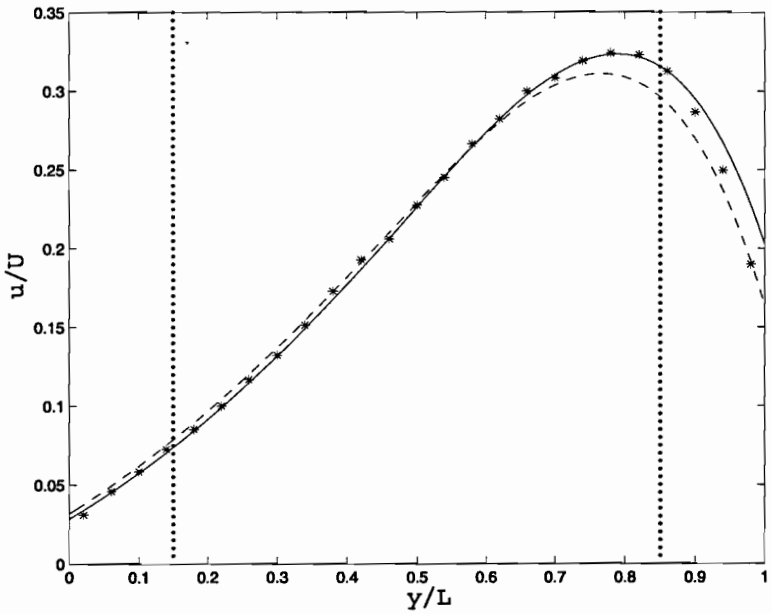

Figure 2. Comparison between Equation (7) (solid line) and DSMC results (stars) for Kn = 0.1, $\phi = 5/\sqrt{2}$. A first-order slip solution is given by the dashed line. The vertical dotted lines enclose the region where a direct comparison between the DSMC (u) and the NS ($\hat{u}$) results is meaningful.

At Kn = 0.4, $\phi = 1.25/\sqrt{2}$, kinetic effects are significant throughout the physical domain. At this Knudsen number the domain size is only 2.5 mean free paths wide and thus u_{KN} is expected to be important everywhere (even if a Knudsen layer is now difficult to define.). This is verified by Figure 4. However, Table 1 shows that the average velocity calculated using Equation (3), which takes the effect of the Knudsen layer into account, is still in excellent agreement with DSMC results up to Kn = 0.4. This leads us to conclude that the second-order slip solution accurately captures the Navier-Stokes component of the flow, which is all that is expected from this solution. In other words, the second-order slip solution is still accurate. At the same time, the first-order slip model significantly underestimates the amount of slip in this solution (see Figure 4). Note that the comparison of Table 1 does not reflect the true difference between the first and

Table 1. Average velocity at $t = \frac{T}{2}$. u_b is calculated using Equation (3)

Kn	u_b/U	u_b^{DSMC}/U
0.1	0.196 (0.196)	0.200
0.2	0.221 (0.216)	0.228
0.4	0.127 (0.112)	0.127

The numbers in parentheses are for the first-order slip model for which no Knudsen layer correction has been applied (see text for discussion).

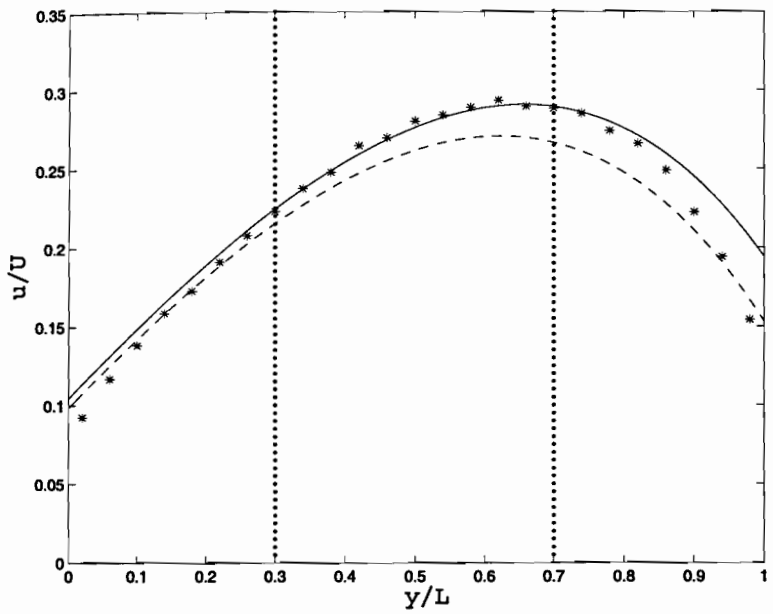

Figure 3. Comparison between Equation (7) (solid line) and DSMC results (stars) for Kn $= 0.2$, $\phi = 2.5/\sqrt{2}$. The first-order slip solution is given by the dashed line. The vertical dotted lines enclose the region where a direct comparison between the DSMC solution (u) and the NS results ($\hat{u}$) is meaningful.

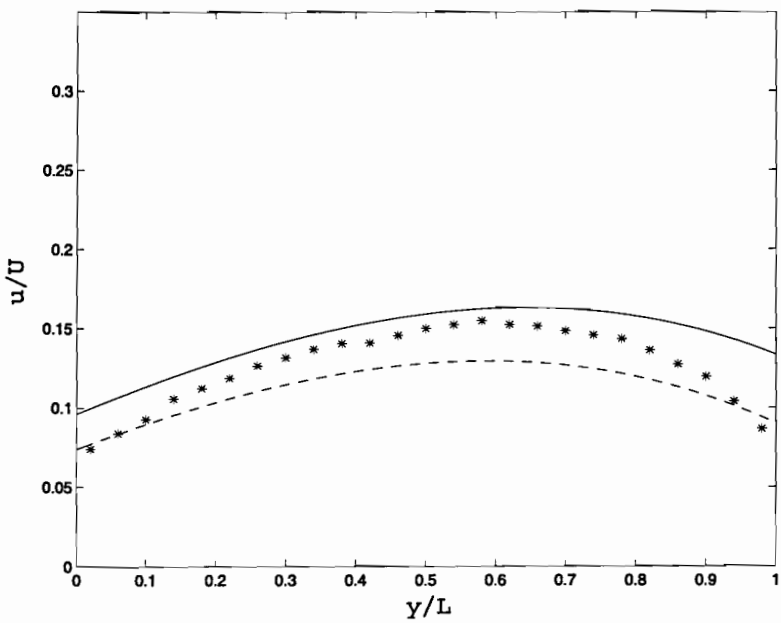

Figure 4. Comparison between Equation (7) (solid line) and DSMC results (stars) for Kn $= 0.4$, $\phi = 1.25/\sqrt{2}$. The first-order slip solution is given by the dashed line. This figure demonstrates that at Kn $= 0.4$ the domain width (2.5λ) is smaller than the combined width of the two Knudsen layers, making a direct comparison between DSMC (u) and the NS results ($\hat{u}$) not useful.

Table 2. Normalized shear stress at the walls at $t = \frac{T}{2}$

Kn	$\lvert\tau_w^*\rvert_{y=0}^{NS}$	$\lvert\tau_w^*\rvert_{y=0}^{DSMC}$	$\lvert\tau_w^*\rvert_{y=L}^{NS}$	$\lvert\tau_w^*\rvert_{y=L}^{DSMC}$
0.1	0.27 (0.29)	0.28 ± 0.02	1.33 (1.48)	1.39 ± 0.04
0.2	0.45 (0.45)	0.43 ± 0.02	0.62 (0.69)	0.62 ± 0.02
0.4	0.18 (0.17)	0.18 ± 0.01	0.175 (0.2)	0.18 ± 0.01

NS denotes the second-order slip model. The numbers in parentheses are for the first-order slip model.

second-order slip models, as evident in Figures 2, 3, and 4, because while the first-order model clearly underestimates the amount of slip present and also neglects the effect of the Knudsen layer, these two sources of error tend to partially cancel each other out. Thus, although the error in the prediction of the average velocity in Table 1 seems to be moderate, in fact the prediction of the first-order slip model is clearly not acceptable for Kn > 0.1. In contrast, the second-order slip model obtains an accurate estimate for the average velocity by correctly capturing the amount of slip and the effect of the Knudsen layer.

In Table 2 we compare the magnitude of the stress at the two walls predicted by the slip-corrected NS description and DSMC. This is an important test, not only because the shear stress is a quantity of interest for this problem (determines the power dissipation), but because it tests the very basis of a slip model, namely that the viscous constitutive relation is valid throughout the physical domain. The nondimensional shear stress τ_w^* at the wall is given by $\tau_w/(\mu U/L)$, where τ_w is the shear stress at the wall. All values are given at $t = \frac{T}{2}$. This table shows that the error in the stress is small even for Kn $= 0.4$. Interestingly, the first-order slip model performs reasonably well.

THE IMPULSIVE START PROBLEM

In this section we evaluate the slip model for a second time-dependent flow. In this case stress fields throughout the flow domain and the mean flow speed as a function of time are investigated in order to gain a better understanding of the limits of validity of the slip model. We consider a dilute gas between two infinitely long, fully accommodating walls; both walls start moving at time $t = 0$ in their plane with velocity U and in the same direction. The governing equation is again Equation (4). Due to the symmetry of the problem we solve Equation (4) in the region $0 \leq y \leq \frac{L}{2}$ using a finite difference method with boundary conditions

$$\hat{u} - U = \alpha\lambda\frac{\partial\hat{u}}{\partial y} - \beta\lambda^2\frac{\partial^2\hat{u}}{\partial y^2} \quad \text{at} \quad y = 0$$

and

$$\frac{\partial\hat{u}}{\partial y} = 0 \quad \text{at} \quad y = \frac{L}{2}$$

Figures 5, 6, and 7 show a comparison between the first- and second-order slip flow solutions and DSMC simulations for Kn $= 0.21$. We clearly see that the local

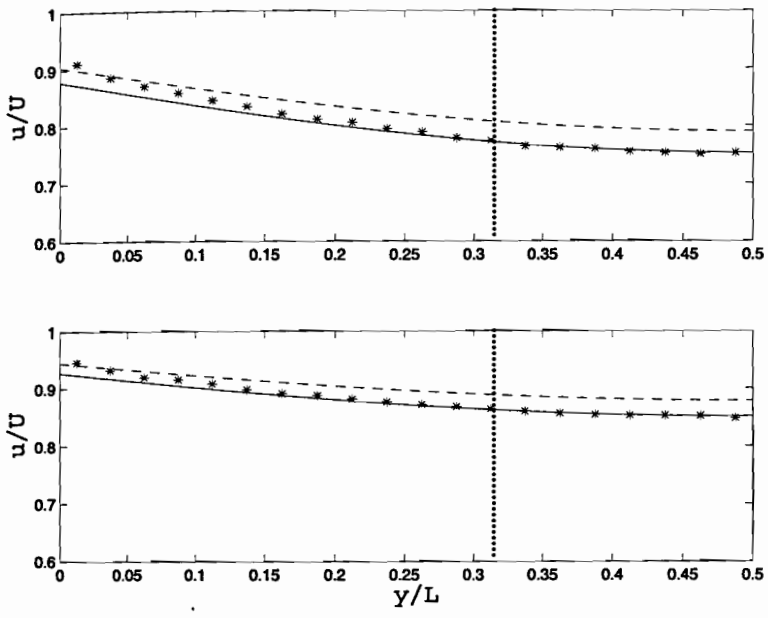

Figure 5. Velocity field comparison for Kn $= 0.21$ at times $16.2\varepsilon^{-1}$ (top) and $21.3\varepsilon^{-1}$ (bottom). The second-order slip solution is shown by the solid line and DSMC simulations by the stars. The first-order slip solution is given by the dashed line. A meaningful comparison between DSMC (u) and NS ($\hat{u}$) results can only be performed to the right of the vertical line ($u_{KN} \to 0$).

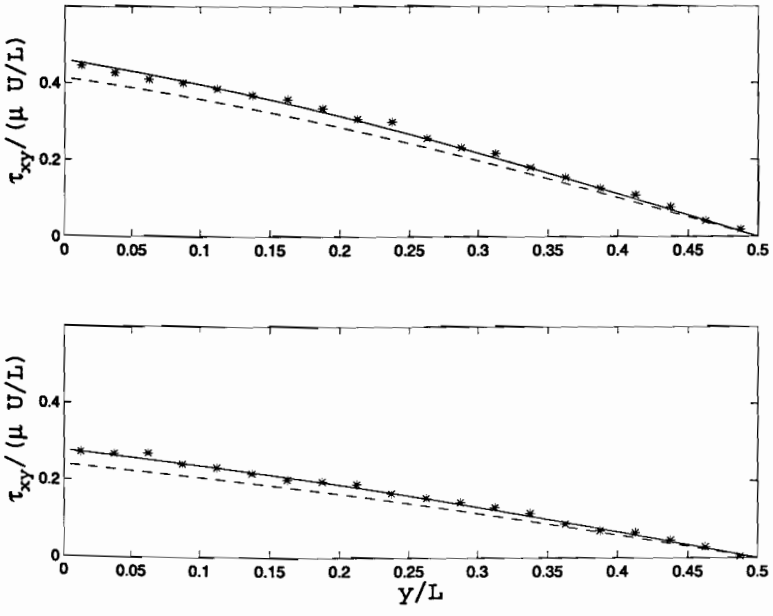

Figure 6. Stress field comparison for Kn $= 0.21$ at times $16.2\varepsilon^{-1}$ (top) and $21.3\varepsilon^{-1}$ (bottom). The second-order slip solution is shown by the solid line and DSMC simulations by the stars. The first-order slip solution is given by the dashed line.

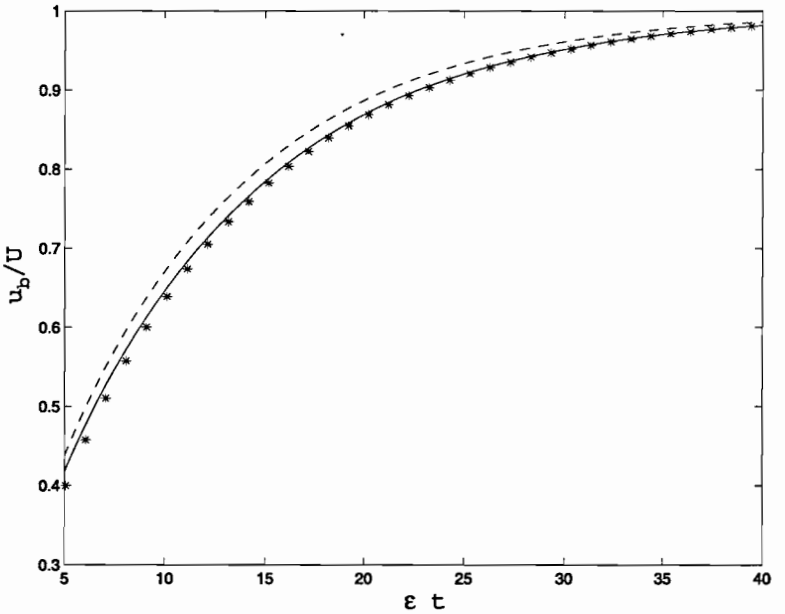

Figure 7. Bulk velocity comparison for Kn = 0.21. The second-order slip solution is shown by the solid line and DSMC simulations by the stars. The first-order slip solution is given by the dashed line.

curvature is important in determining the deviation between the DSMC and second-order NS result in the Knudsen layer again delimited by the vertical line in Figure 5. This deviation, however, as before, does not reflect a failure of the second-order slip model. Figures 6 and 7 clearly show that the stress field and average velocity are accurately captured by the second-order slip model. The first-order slip model captures the stress field with qualitative accuracy, it does not predict the time history of the average velocity accurately. In fact, as noted before, the existence of the Knudsen layer (see Figure 5) makes the first-order slip model look better than it actually is.

Figures 8, 9, and 10 show that at Kn = 0.31 the second-order slip model remains accurate, while the Knudsen layer covers essentially the whole domain. The first-order slip description is less accurate.

Figures 11, 12, and 13 show a comparison at Kn = 0.42. Clearly, the discrepancy in the velocity is significant but this is mainly due to the role of the Knudsen layer explained above. The true error can be judged in Figures 12 and 13 and can be seen to be of the order of a few percent (at Kn = 0.42), suggesting that may be the limit of applicability of this model for one-dimensional flows. This level of error may be adequate for engineering-type calculations, especially considering the computational cost associated with solutions of the Boltzmann equation.

CONCLUSIONS

We have presented a comparison between a recently proposed second-order slip model and DSMC simulations for two time-dependent problems. These particular problems were chosen due to their practical importance but also because they provide flow

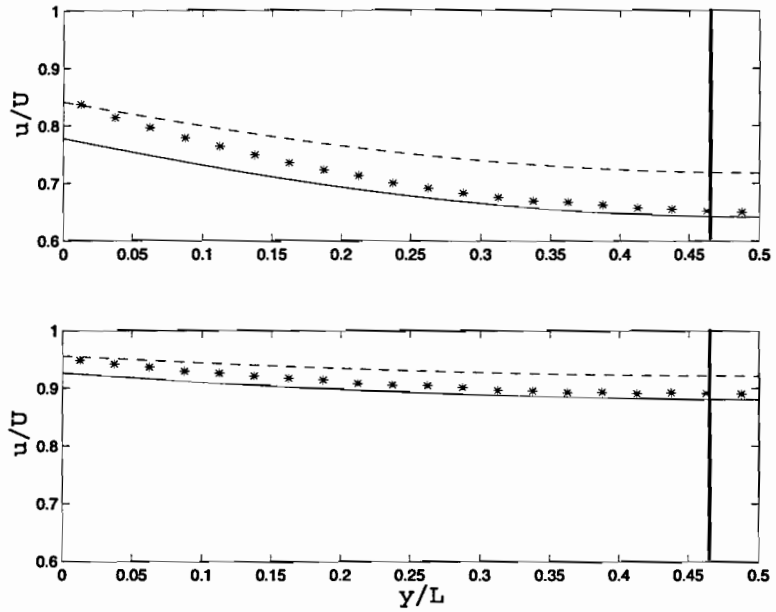

Figure 8. Velocity field comparison for Kn = 0.31 at times $7.5\varepsilon^{-1}$ (top) and $14.2\varepsilon^{-1}$ (bottom). The second-order slip solution is shown by the solid line and DSMC simulations by the stars. The first-order slip solution is given by the dashed line. A meaningful comparison between DSMC (u) and NS ($\hat{u}$) results can only be performed to the right of the vertical line ($u_{KN} \to 0$).

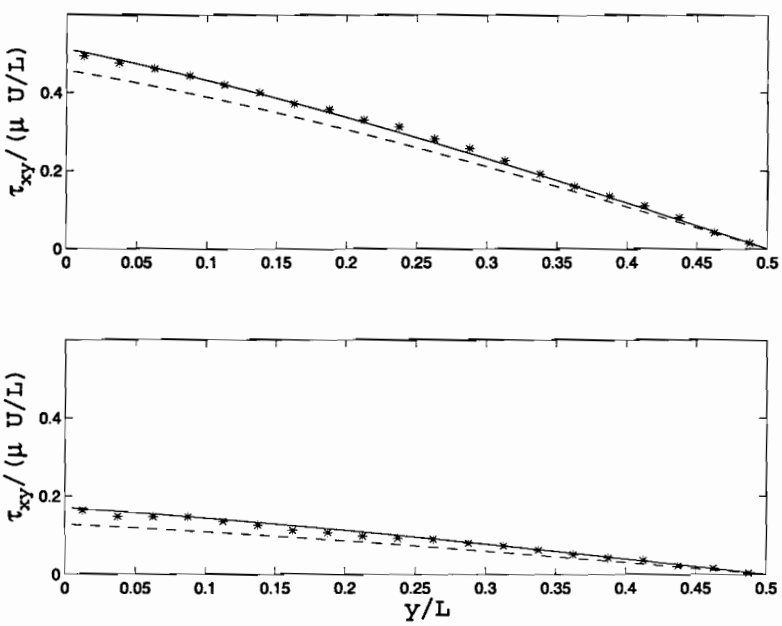

Figure 9. Stress field comparison for Kn = 0.31 at times $7.5\varepsilon^{-1}$ (top) and $14.2\varepsilon^{-1}$ (bottom). The second-order slip solution is shown by the solid line and DSMC simulations by the stars. The first-order slip solution is given by the dashed line.

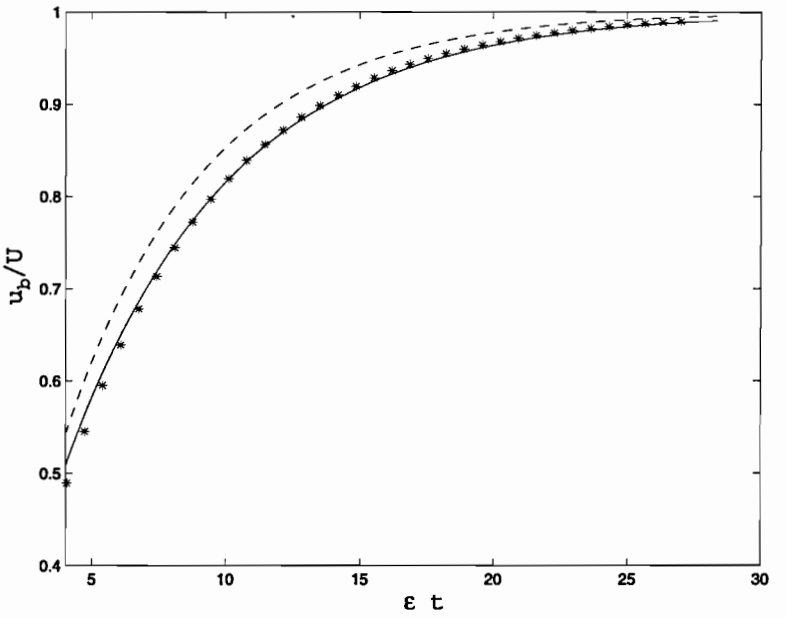

Figure 10. Bulk velocity comparison for Kn = 0.31. The second-order slip solution is shown by the solid line and DSMC simulations by the stars. The first-order slip solution is given by the dashed line.

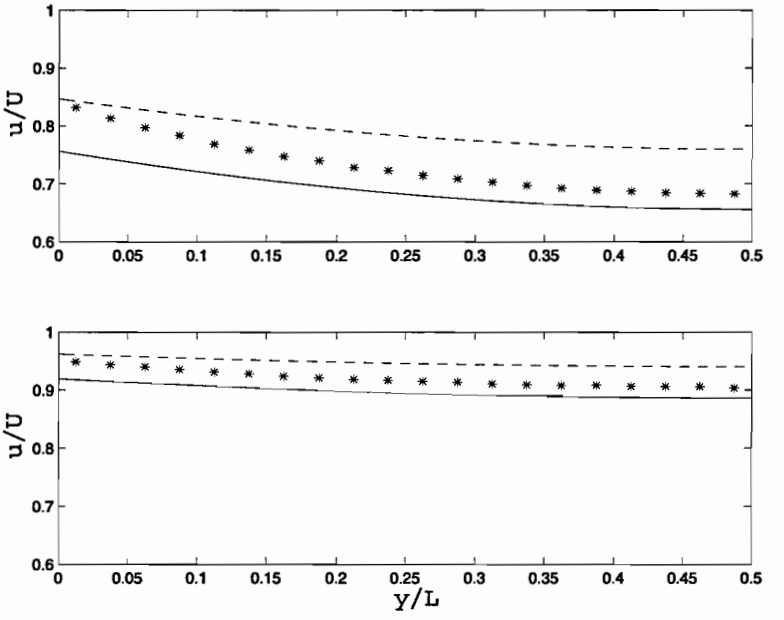

Figure 11. Velocity field comparison for Kn = 0.42 at times $5.6\varepsilon^{-1}$ (top) and $10.7\varepsilon^{-1}$ (bottom). The second-order slip solution is shown by the solid line and DSMC simulations by the stars. The first-order slip solution is given by the dashed line. Note that the Knudsen layer width is larger than the half domain shown here so a direct comparison is not very useful.

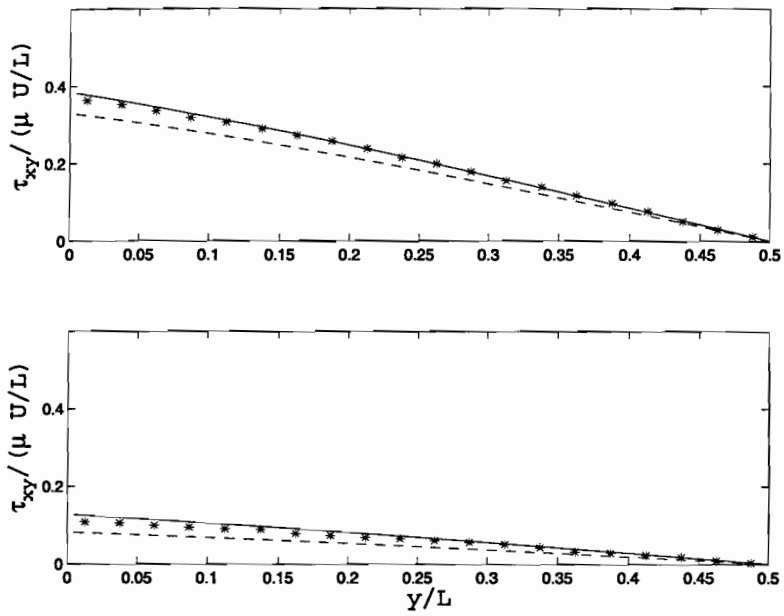

Figure 12. Stress field comparison for Kn = 0.42 at times $5.6\varepsilon^{-1}$ (top) and $10.7\varepsilon^{-1}$ (bottom). The second-order slip solution is shown by the solid line and DSMC simulations by the stars. The first-order slip solution is given by the dashed line.

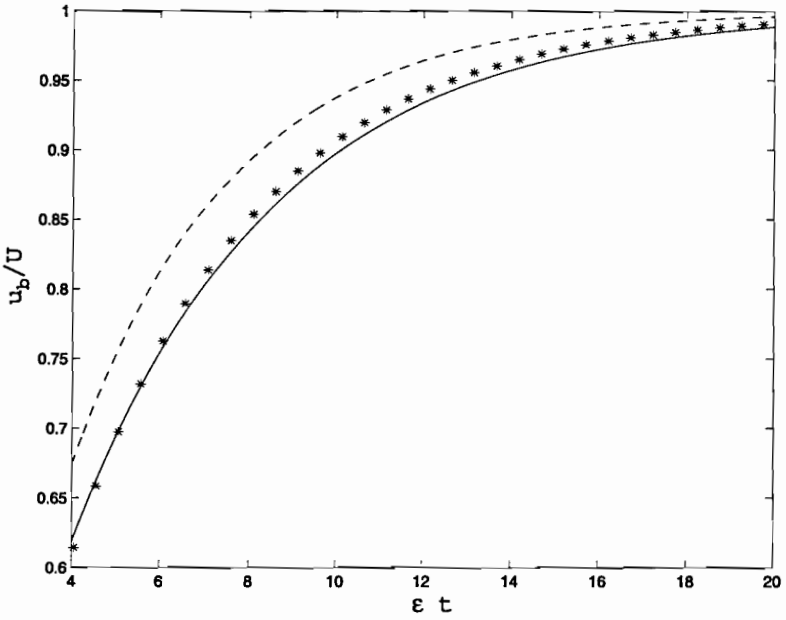

Figure 13. Bulk velocity comparison for Kn = 0.42. The second-order slip solution is shown by the solid line and DSMC simulations by the stars. The first-order slip solution is given by the dashed line.

fields that are quantitatively different from the steady, pressure-driven flow for which the second-order model has been previously tested. The transient nature of these flows also provides a more stringent test of the model.

Our discussion illustrates the capabilities but also the limitations of a rigorous second-order slip model. The Knudsen layer, an integral part of the asymptotic analysis that leads to the slip-flow description, becomes sufficiently important to hold the key to not only developing a predictive slip model but also interpreting and using the latter's predictions. Our results show that the second-order slip model provides very good approximations to the actual flow well into the transition regime provided that the Knudsen layer is properly accounted for. More specifically, the model is accurate at distances from the wall that exceed 1.5λ, while for smaller distances it provides a baseline to which the contribution of the Knudsen layer can be added. The slip model also predicts the stress field accurately with no adjustable parameters. In contrast, a first-order slip model clearly significantly underestimates the amount of slip present in the flow starting from as early as $\mathrm{Kn} \cong 0.1$. Regarding the stress field, the first-order model performs well in a qualitative sense but is again significantly less accurate compared to the second-order model. In the case of the average flow velocity in particular, where the effect of the Knudsen layer can be directly accounted for, the first-order slip model performs rather poorly but the fortuitous cancellation between the second-order slip and the flow deficit due to the Knudsen layer for $\mathrm{Kn} > 0.1$ tends to flatter its performance.

It appears that the steady assumption under which the second-order slip model was derived can be lifted, presumably as long as the flow timescale is long compared to the molecular collision time. Although the exact Knudsen number beyond which this model should not be used depends on the acceptable error lever, and, perhaps, on the particular problem characteristics such as dimensionality and flow field complexity, our results indicate that this model can be reliably used up to $\mathrm{Kn} \cong 0.4$, at least for one-dimensional problems. Given the significant computational advantage of the NS formulation compared to the Boltzmann equation and the gradual deterioration in accuracy [7] this slip model exhibits, the latter model may prove to be useful for preliminary calculations well beyond $\mathrm{Kn} \cong 0.4$ although the complexity of slip models in higher dimensions [6] may make it less attractive.

REFERENCES

1. N. G. Hadjiconstantinou, Sound Propagation at Small Scales under Continuum and Non-Continuum Transport, *Journal of Fluid Mechanics*, vol. 488, pp. 399–408, 2003.
2. N. G. Hadjiconstantinou and O. Simek, Constant-Wall-Temperature Nusselt Number in Micro and Nano-Channels, *Journal of Heat Transfer*, vol. 124, pp. 356–364, 2002.
3. G. M. Karniadakis and A. Beskok, *Micro Flows: Fundamentals and Simulation*, New York: Springer, 2002.
4. C. Cercignani, *Higher Order Slip According to the Linearized Boltzmann Equation*, Institute of Engineering Research Report AS-64-19, University of California, Berkeley, 1964.
5. T. Ohwada, Y. Sone, and K. Aoki, Numerical Analysis of the Shear and Thermal Creep Flows of a Rarefied Gas over a Plane Wall on the Basis of the Linearized Boltzmann Equation for Hard-Sphere Molecules *Physics of Fluids*, vol. 1, pp. 1588–1599, 1989.
6. Y. Sone, *Kinetic Theory and Fluid Dynamics*, Boston: Birkhäuser, 2002.
7. N. G. Hadjiconstantinou, Comment on Cercignani's Second-Order Slip Coefficient, *Physics of Fluids*, vol. 15, no. 8, pp. 2352–2354, 2003.

8. J. Maurer, P. Tabeling, P. Joseph, and H. Willaime, Second-Order Slip Laws in Microchannels for Helium and Nitrogen, *Physics of Fluids*, vol. 15, pp. 2613–2621, 2003.
9. C. Cercignani, *The Boltzmann Equation and Its Applications*, Springer-Verlag, New York, 1988.
10. G. A. Bird, *Molecular Gas Dynamics and the Direct Simulation of Gas Flows*, Clarendon Press, Oxford, 1994.
11. N. G. Hadjiconstantinou, Sound Wave Propagation in Transition-Regime Micro- and Nanochannels, *Physics of Fluids*, vol. 14, no. 2, pp. 802–809, 2002.
12. W. Wagner, A Convergence Proof for Bird's Direct Simulation Monte Carlo Method for the Boltzmann Equation, *Journal of Statistical Physics*, vol. 66, pp. 1011–1044, 1992.
13. F. Alexander, A. L. Garcia, and B. Alder, Cell Size Dependence of Transport Coefficients in Stochastic Particle Algorithms, *Physics of Fluids*, vol. 10, pp. 1540–1542, 1998; Erratum: *Physics of Fluids*, vol. 12, p. 731, 2000.
14. N. G. Hadjiconstantinou, Analysis of Discretization in the Direct Simulation Monte Carlo, *Physics of Fluids*, vol. 12, pp. 2634–2638, 2000.
15. A. L. Garcia and W. Wagner, Time Step Truncation Error in Direct Simulation Monte Carlo, *Physics of Fluids*, vol. 12, pp. 2621–2633, 2000.
16. P. Bahukudumbi, J. H. Park, and A. Beskok, A Unified Engineering Model for Steady and Unsteady Shear-Driven Gas Microflows, *Microscale Thermophysical Engineering*, vol. 7, pp. 291–315, 2003.
17. J. H. Park, P. Bahukudumbi, and A. Beskok, Rarefaction Effects on Shear Driven Oscillatory Gas Flows: A DSMC Study in the Entire Knudsen Regime, *Physics of Fluids*, vol. 16, pp. 317–330, 2004.
18. N. G. Hadjiconstantinou, A. L. Garcia, M. Z. Bazant, and G. He, Statistical Error in Particle Simulations of Hydrodynamic Phenomena, *Journal of Computational Physics*, vol. 187, no. 1, pp. 274–297, 2003.
19. N. G. Hadjiconstantinou, Oscillatory Shear-Driven Gas Flows in the Transition and Free-Molecular Flow Regimes, to appear in *Physics of Fluids*, 2005.
20. T. Ohwada, Y. Sone, and K. Aoki, Numerical Analysis of the Poiseuille and Thermal Transpiration Flows Between Two Parallel Plates on the Basis of the Boltzmann Equation for Hard-Sphere Molecules, *Physics of Fluids A*, vol. 1, no. 12, pp. 2042–2049, 1989.

MICROSCALE THERMOPHYSICAL ENGINEERING

Abstracted/indexed in: Applied Mechanics Review; Current Contents/Engineering, Computing, and Technology; Current Contents/Physical, Chemical and Earth Sciences; Institut de L'Information Scientifique et Technique (INIST); Materials Science Citation Index; Research Alert; SciSearch.

Microscale Thermophysical Engineering (USPS permit number 020-938) is published quarterly in February, May, August, and November by Taylor & Francis, Inc., 325 Chestnut Street, Philadelphia, PA 19106. Periodicals postage paid at Philadelphia, PA and additional mailing offices.

US Postmaster: Please send address changes to UMTE c/o IMS, PO Box 1518, Champlain, NY 12919, USA.

Annual Subscription, Volume 9, 2005

Print ISSN – 1089-3954 Online ISSN – 1091-7640

Institutional subscribers: $675 (US), £409 (UK).

Personal subscribers: $238 (US), £144 (UK).

An institutional subscription to the print edition includes free access to the online edition for any number of concurrent users across a local area network.

Production and Advertising Office: 325 Chestnut Street, Philadelphia, PA 19106. Tel - 215-625-8900, Fax - 215-625-8563. Production Editor: Andrea McFadden.

Subscription offices

USA/North America: Taylor & Francis Inc., 325 Chestnut Street, Philadelphia, PA 19106. Tel: 215-625-8900, Fax: 215-625-2940.

UK/Europe: Taylor & Francis Ltd., Rankine Road, Basingstoke, Hampshire RG24 8PR, UK. Tel: +44 (0) 1256 813 000, Fax: +44 (0) 1256 330 245.

For a complete guide to Taylor & Francis Group's journal and book publishing programs, visit our website: **www.taylorandfrancis.com.**